

Pressure-induced dimerization and molecular orbitals formation in Na_2RuO_3 with strong correlation-enhanced spin-orbit coupling effect

Xujia Gong,¹ Wei Wang,² Wen Lei,³ Feng Xiao,¹ Carmine Autieri,⁴ Congling Yin,⁵ and Xing Ming^{1,5*}

1. College of Science, Guilin University of Technology, Guilin 541004, PR China

2. School of Materials Science and Engineering, Beihang University, Beijing 100191, PR China

3. Key Laboratory of Artificial Micro- and Nano-Structures of Ministry of Education and School of Physics and Technology, Wuhan University, Wuhan 430072, PR China

4. International Research Centre MagTop, Institute of Physics, Polish Academy of Sciences, Aleja Lotników 32/46, PL-02668 Warsaw, Poland

5. MOE Key Laboratory of New Processing Technology for Nonferrous Metal and Materials, Guangxi Key Laboratory of Optic and Electronic Materials and Devices, Guilin University of Technology, Guilin 541004, PR China

ABSTRACT

First-principles calculations and simulations are conducted to clarify the nonmagnetic insulating ground state of the honeycomb lattice compound Na_2RuO_3 with $4d^4$ electronic configuration and explore the evolutions of crystal structure and electronic property under pressure. We reveal that individual Coulomb correlation or spin-orbit coupling (SOC) effect cannot reproduce the experimentally observed nonmagnetic insulating behavior of Na_2RuO_3 , whereas the Coulomb correlation enhanced SOC interactions give rise to an unusual spin-orbital-entangled $\mathbf{J} = 0$ nonmagnetic insulating state, which contrasts with the SOC assisted Mott insulating state in d^5 ruthenates and iridates. Furthermore, a pressure-induced structural dimerization transition has been predicted around 15-17.5 GPa. The honeycomb lattice of the high-pressure dimerized phase features with parallel pattern of the short Ru-Ru dimers aligning along the crystallographic b -axis direction. Accompanied with the structural dimerization, the electronic structure shows striking reconstruction by formation of molecular orbitals. Interestingly, the cooperation of Coulomb correlation together with SOC can realize a nonmagnetic insulating state in the high-pressure dimerized phase. The d^4 ruthenate Na_2RuO_3 with honeycomb lattice will provide a new platform to explore unusual physics and rich phase diagram due to the delicate interplay of lattice degree of freedom, electron correlations, and SOC interactions.

* Email: mingxing@glut.edu.cn (Xing Ming)

I. INTRODUCTION

The competition between spin-orbit coupling (SOC), Coulomb correlations together with Hund's coupling interactions has given rise to a rich set of emergent phenomena and exotic quantum states in $4d/5d$ transition metals compounds [1-4]. Particularly, the seminal discovery of the SOC-induced Mott insulating state in the iridate Sr_2IrO_4 [5] has sparked considerable enthusiasm to explore unprecedented spin-orbital-entangled phases [6-8]. The spin-orbital-entangled j_{eff} states become indispensable ingredients to understand the exotic electronic structures and magnetic properties of ruthenates and iridates [1-8].

Recently, the ruthenates and iridates with d^4 electronic configuration have attracted tremendous interest due to their rich phase diagram and potential excitonic magnetism [7,9-12]. According to the prevailing wisdom of the j_{eff} picture in the strong SOC limit, the t_{2g} states of the $4d$ and $5d$ orbital will split into effective $j_{\text{eff}} = 1/2$ doublet and $j_{\text{eff}} = 3/2$ quartet by SOC splitting [1,5,7]. Therefore, all the four electrons of the d^4 ions with t_{2g}^4 electronic configuration are anticipated to fully occupy the lower-energy $j_{\text{eff}} = 3/2$ states, which are separated from the higher-energy empty $j_{\text{eff}} = 1/2$ states by a gap of $3\lambda/2$ (λ is the SOC strength). As a result, a SOC-induced $\mathbf{J} = 0$ nonmagnetic band insulator (often named as relativistic band insulator) should be obtained naturally. On the other hand, when the electron correlations are dominant over SOC interactions, an alternative scenario of SOC entangled $\mathbf{J} = 0$ nonmagnetic state has been put forward [6,7,11]. According to such a LS -coupling scheme, the low-spin t_{2g}^4 electronic configuration shows total spin $S = 1$ and threefold orbital degeneracy with an effective orbital moment $\mathbf{L} = 1$, then the intra-atomic SOC interactions give rise to a Van Vleck-type nonmagnetic $\mathbf{J} = 0$ singlet by antiparallel alignment of the spin and orbital angular momentum. Based on such a SOC-driven nonmagnetic $\mathbf{J} = 0$ ground state in $4d/5d$ compounds with d^4 electron configuration, theoretical predictions anticipate novel excitonic magnetism may be realized due to the condensation of spin-orbital $\mathbf{J} = 1$ triplons [11]. However, attributed to the delicate balance of comparable energy scales of SOC, Coulomb interaction, Hund's Coupling, and non-cubic crystal field splitting, breakdown of the $\mathbf{J} = 0$ nonmagnetic state and resultant complicated magnetic behavior have been extensively uncovered in real materials [7]. The $\mathbf{J} = 0$ non-magnetic ground state in $4d/5d$ compounds with d^4 electron configuration has been a controversial topic still under intense debate. For instance, conflicting magnetic behaviors for double-perovskite iridates Sr_2YIrO_6 and Ba_2YIrO_6 are reported in both

experimental and theoretical studies [13-18]. The origin of these controversial magnetic properties is still ambiguous. Recent experimental works support the $J = 0$ ground state for the Ir^{5+} oxides A_2BIrO_6 (A= Ba, Sr; B= Lu, Sc), $\text{Sr}_3\text{NaIrO}_6$ and $\text{Sr}_3\text{AgIrO}_6$, and indicate that the magnetic signals are from extrinsic sources, such as magnetic impurities or antisite disorder [19-22].

Alternately, the tetravalent ruthenates (Ru^{4+} , $4d^4$) A_2RuO_3 (A = Na, Li) [23-29] and $\text{Ag}_3\text{LiRu}_2\text{O}_6$ [30,31] feature with a nearly ideal honeycomb lattice and weaker SOC strength relative to iridates, which provides a new playground to explore unusual physics emerging from the intricate interplay of electron correlations, SOC and Hund's Coupling. A nonmagnetic state has been found in Li_2RuO_3 under ambient conditions, which is not related to the spin-orbital-entangled $J = 0$ state but rather associated with structural dimerization of the honeycomb lattice and molecular orbital formation in the Ru-Ru dimer [23,24]. In contrast to the distorted honeycomb structure with an armchair pattern of the long/short Ru-Ru bonds in Li_2RuO_3 [23-27], Na_2RuO_3 [28,29] and $\text{Ag}_3\text{LiRu}_2\text{O}_6$ [30,31] crystallize in a nearly perfect honeycomb lattice with almost equal Ru-Ru bond lengths, which may serve as model systems to study spin-orbital-entangled $J = 0$ physics. However, contradictory magnetism including antiferromagnetic (AFM) coupling interactions between the Ru moments and spin-orbital-entangled nonmagnetic singlet state has been observed experimentally in $\text{Ag}_3\text{LiRu}_2\text{O}_6$ at ambient pressure [30,31]. R. Kumar *et al.* studied the unconventional magnetism of $\text{Ag}_3\text{LiRu}_2\text{O}_6$, where the magnetic susceptibility $\chi(T)$ data shows a strong AFM coupling between the Ru moments without any anomaly down to 2 K, but the neutron diffraction does not detect any magnetic order down to 1.6 K [30]. In contrast, T. Takayama *et al.* performed magnetic and spectroscopic measurements, together with the quantum chemistry calculation, indicating that $\text{Ag}_3\text{LiRu}_2\text{O}_6$ is a Mott insulator and hosts a spin-orbit-entangled nonmagnetic $J = 0$ singlet [31]. In addition, conflicting measurement results of electrical transport properties and magnetic properties have also been reported for Na_2RuO_3 . Firstly, the resistance measurements show insulating behavior, which contradicts the metallic behavior observed in the photoelectron spectroscopy measurements, where the synthesized polycrystalline samples of Na_2RuO_3 consisted of ~94% ordered phase and ~6% disordered phase of Na_2RuO_3 [32]. However, the Arrhenius fitting of resistivity data as well as x-ray absorption and emission spectra give an activation energy of 80 meV for the disordered phase of Na_2RuO_3 , indicating very small gap [33]. In contrast, M. Tamaru *et al.* claimed that the disordered phase of Na_2RuO_3 shows metallic conduction [34]. Secondly, Wang *et al.* claimed that

they have synthesized single crystals of Na_2RuO_3 and found it to be a semiconducting antiferromagnet with a Néel temperature around 30 K from bulk susceptibility and heat-capacity measurements [29]. However, it was suspected that the single crystals from their study have been mistakenly assigned to Na_2RuO_3 , because the features of the susceptibility and heat capacity in this work are remarkably similar to those observed in Na_3RuO_4 [35]. In contrast, Veiga *et al.* [32] observed no sign of magnetic ordering or magnetic frustration down to 1.5 K, where the magnetic susceptibility $\chi(T)$ is weakly temperature-dependent and is likely dominated by the Pauli term above 50 K. The low-temperature Curie-Weiss contribution is equivalent to approximately 10% by mass of the $S = 1$ impurity, and the disordered phase (~6% weight percentage of the as synthesized samples) might be responsible for the magnetic impurities. Particularly, an estimated intrinsic susceptibility χ_0 obtained by subtracting a Curie-like $1/T$ contribution is almost temperature-independent. Actually, the magnetic susceptibility of Na_2RuO_3 is very similar to that of K_2RuCl_6 , another ruthenate with d^4 electron configuration, which features a characteristic of the Van Vleck paramagnetic susceptibility of isolated $J = 0$ ions [36]. Furthermore, inelastic neutron scattering experiments observe nonmagnetic behavior rather than any sign of long-range magnetic ordering for Na_2RuO_3 [37]. The discrepancies between these previous works are perhaps originated from the different samples and the ordered or disordered polymorphs of Na_2RuO_3 . According to previous experimental reports, Na_2RuO_3 crystallizes in two polymorphs, one is a disordered phase with $R\bar{3}m$ space group, another one is the ordered phase with $C2/m$ space group [28,38,39]. As a result, the x-ray diffraction patterns differ a bit that the ordered phase has diffuse scatterings arising from the honeycomb ordering in the $[\text{Na}_{1/3}\text{Ru}_{2/3}]\text{O}_2$ slabs. The ordered and disordered polymorphs exhibit significant differences in the electrochemical performances [38]. A comprehensive study of the bulk properties of single pure-phase ordered or disordered polymorphs of Na_2RuO_3 is highly required.

The conflicting and complicated magnetic properties in the d^4 ruthenates with honeycomb lattice point to an interesting possibility of realizing novel phases near the quantum critical point, which can be driven by doping, strain, or pressure [6,40]. However, $\text{Ag}_3\text{LiRu}_2\text{O}_6$ displays successive pressure-induced structural transitions and remains nonmagnetic behavior rather than excitonic magnetism [31]. Density functional theory (DFT) calculations predict a pressure-induced structural transition from the idea honeycomb lattice (space group $C2/m$) to a dimerized structure (space group $P2_1/m$) for the ordered phase Na_2RuO_3 at ~3 GPa [41]. In spite of the theory-predicted transition

pressure of 3 GPa is easily accessible, the structural transition has not been confirmed experimentally yet. Furthermore, ignoring the electronic correlations and SOC interactions, electronic structure calculations indicate that Na_2RuO_3 showing metallic characteristics before and after the structural transition, which are inconsistent with recently observed nonmagnetic insulating behavior in the ordered phase Na_2RuO_3 [32,37].

The conflicting experimental results raise a question of whether a spin-orbital-entangled state can provide a suitable description for the nonmagnetic insulating behavior of the ordered phase Na_2RuO_3 . Furthermore, it is imperative to reevaluate the structural stability of Na_2RuO_3 under pressure because previous prediction of the pressure-induced dimerized transition for the ordered phase Na_2RuO_3 at 3 GPa is still unverified by experiment. In the present work, we revisit the electronic structure of the ordered phase Na_2RuO_3 under ambient conditions by explicitly considering the Coulomb interactions and SOC, and explore the evolution of the honeycomb lattice and electronic structure as a function of applied pressure by first-principles calculations based on DFT. The calculated results indicate that only SOC interactions combined with Coulomb repulsion can give rise to the insulating nonmagnetic ground state of the ordered phase Na_2RuO_3 . Furthermore, we predict a pressure-induced structural dimerization at 17.5 GPa, which is accompanied with electronic structure transformations and the emergence of molecular orbital. The crucial role of Coulomb correlation conspiring with SOC interactions in the honeycomb lattice ruthenate Na_2RuO_3 provides a good platform to study the spin-orbital-entangled physics. These theoretical results will attract further experimental confirmation of pressure-induced dimerization as well as electronic structure transition from the nonmagnetic insulating spin-orbital-entangled state to molecular orbitals state.

II. STRUCTURE MODEL AND COMPUTATIONAL DETAILS

The crystal structures of Na_2RuO_3 have been characterized with an ordered phase in monoclinic space group $C2/m$ or $C2/c$ and a disordered phase in rhombohedral space group $R\bar{3}m$ [28,32,38,39]. The Na and Ru ions are randomly distributed in the $[\text{Na}_{1/3}\text{Ru}_{2/3}]\text{O}_2$ slabs in the disordered phase, whereas the ordered phase features with a honeycomb-ordered $[\text{Na}_{1/3}\text{Ru}_{2/3}]\text{O}_2$ slabs. As shown in **FIG. 1(a)**, the edge-sharing RuO_6 octahedra form hexagons with Na ions in the cavity, and the hexagons share edge to form a quasi-two-dimensional honeycomb $[\text{Na}_{1/3}\text{Ru}_{2/3}]\text{O}_2$ slabs intercalated with Na ions in the interlayer spacing. Among the six Ru-Ru bonds of one hexagon, two (four) of

them are labeled as X (Y), X and Y bonds are almost the same according to experimentally characterized lattice parameters ($1-X/Y = -0.000734$) (FIG. 1(b)). The tiny differences of the X and Y bonds lead to small deviations of the hexagon interior angles ($\alpha_1 = 120.022^\circ$ and $\alpha_2 = 119.956^\circ$) from the case of ideal regular hexagon of 120° . As the sister compound of Na_2RuO_3 , Li_2RuO_3 crystallizes in $C2/m$ space group above $T_c = 540$ K, which transform to $P2_1/m$ space group below T_c [23]. Although the space groups of $C2/m$ and $C2/c$ differ a bit, our calculated results indicate that their energies are almost the same (detailed lattice parameters and energies can be found in Table S1 in the Supplemental Material [42], and the corresponding atomic positions of Na_2RuO_3 were tabulated in Tables S2-S4). In addition, we also optimized the structure with $P2_1/m$ space group by substitution Li atoms in Li_2RuO_3 with Na [23], but it has a higher energy and a dimerized Y bond (2.695 Å). Obviously, the dimerized structure with $P2_1/m$ space group is inconsistent with the non-dimerized phase of the ordered phase Na_2RuO_3 observed at ambient conditions. According to the most recent experimental reported results [39], the ordered monoclinic phases of Na_2RuO_3 with $C2/m$ space group will be employed in further simulation process.

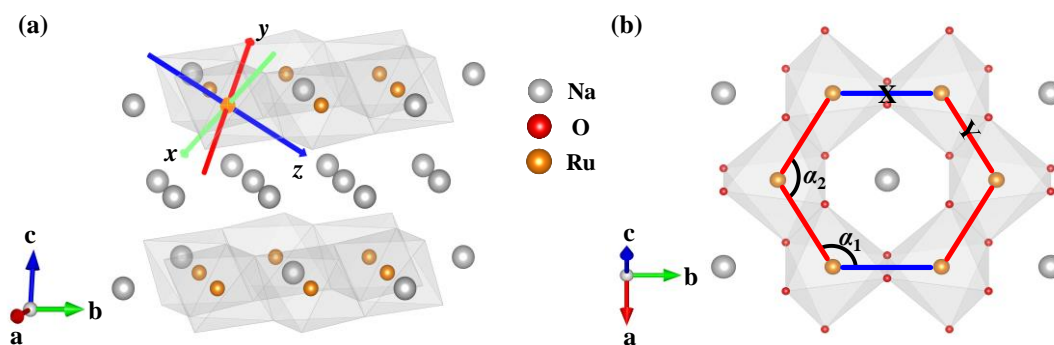


FIG. 1. (a) Conventional cell of the ordered phase Na_2RuO_3 with honeycomb-ordered $[\text{Na}_{1/3}\text{Ru}_{2/3}]\text{O}_2$ slabs. For clarity, the Na/Ru atoms are shown as grey/golden balls, while O atoms at the apexes of RuO_6 octahedra are not shown. We set up a local coordinate system (x, y, z) approximately along three perpendicular O-Ru-O bonds of a RuO_6 octahedron. (b) Schematic diagram of the hexagonal ab plane of the honeycomb Na_2RuO_3 , together with the Ru-Ru bonds (denoted as X (blue) and Y (red) bonds) and interior angles (α_1 and α_2) in the hexagons formed by edge-sharing RuO_6 octahedra.

We performed all of the DFT calculations by employing the projector-augmented wave (PAW) method [43] as implemented in the Vienna *ab initio* simulation package (VASP) [44,45], jointing with the full-potential linearized augmented plane wave (FP-LAPW) method as implemented in the

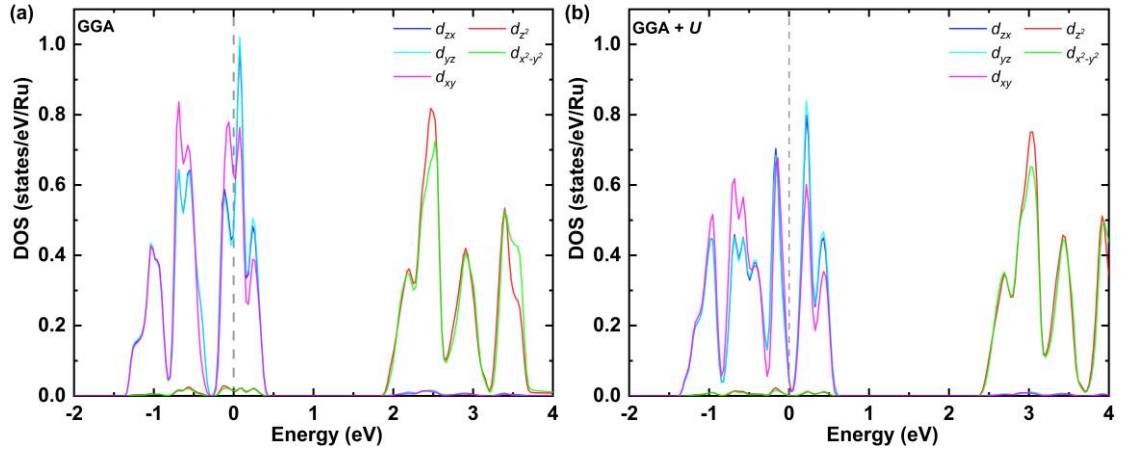
WIEN2K package [46]. The generalized gradient approximation (GGA) proposed by Perdew, Burke and Ernzerhof (PBE) was chosen to describe the exchange correlation potential [47]. On-site Coulomb interaction $U = 3$ eV and the Hund's coupling $J_H = 0.3$ eV (except otherwise specified) for the Ru atoms were used to deal with the electronic correlation by the DFT+ U method introduced by Liechtenstein *et al* [48]. The DFT+ U method has been widely employed to study the nonmagnetic compound with d^4 electronic configuration, such as the K_2OsX_6 ($X=F, Cl, \text{ and } Br$) [49], Li_2RuO_3 [26], $SrIr_2O_6$ [50], $NaIrO_3$ [51]. Especially, the Coulomb correlation interactions (U) play an important role in realizing the insulating band gap of the dimerized honeycomb ruthenate Li_2RuO_3 features with molecular orbitals, and give a reasonable description of the experimental observed anisotropy of the susceptibility [26]. Therefore, the DFT+ U method is suitable to study on Na_2RuO_3 with d^4 electronic configuration. All the structural optimization was carried out by using the VASP code, where the kinetic-energy cutoff was set to 520 eV, and k points spacing was set to $2\pi \times 0.2 \text{ \AA}^{-1}$, while the convergence criteria of total energy and atomic force were set to 10^{-6} eV and 0.01 eV/\AA , respectively. To explore the stability of the honeycomb lattice under pressure, we performed simulations of the structural evolution under compression. The simulation started from the experimental atomic configuration by switching off the symmetry constraints (corresponding to the $P1$ space group) and mimicked the application pressure by gradually increasing the pressure parameter with a step of 2.5 GPa up to 40 GPa. The electronic structures including band structures and density-of-state (DOS) were cross-checked by the VASP and WIEN2K packages.

As shown in **Table S5** [42], the optimization results of the structural parameters at ambient condition within GGA+ U are in better agreement with the experimental data [39], the deviations of lattice parameters from the experimental results after geometry optimization are less than 1.2% at ambient conditions. In contrast, the optimized lattice parameters dramatically deviate from the experimental results when Coulomb interaction U was not considered (see the comparison in **Table S5** [42]). Particularly, the X bond shows very obvious shortening (3.027 \AA) with respect to the Y bonds (3.197 \AA), which is obviously inconsistent with the experimental results of the non-dimerized phase at ambient condition. The agreement between the experimental data at ambient conditions and the theoretically calculated lattice parameters within GGA+ U method confirms the validity of the calculation parameters.

III. RESULTS AND DISCUSSION

A. The nonmagnetic ground state under ambient conditions

The band structures of Na_2RuO_3 under ambient conditions are displayed in **FIG. S1** [42], and the corresponding projection of DOS are presented in **FIG. 2**. As shown in **FIG. S1(a)** and **FIG. 2(a)**, we could not open a band gap when using the standard GGA for our DFT calculation. Though there are structural distortions for the RuO_6 octahedra, the $4d$ orbitals of the Ru^{4+} ions have been split into two-fold degenerate e_g states ($d_{x^2-y^2}$ and d_{z^2}) and three-fold degenerate t_{2g} states (d_{xy} , d_{yz} and d_{zx}). The t_{2g} orbitals span over the Fermi level ranging from -1.3 to 0.4 eV and result in a metallic state, which are separated from the fully empty e_g states by a large crystal-field splitting ($10Dq$). We expect that the insulating gap will be opened by a modest onsite Coulomb repulsion U among the Ru $4d$ states. Regrettably, although the electronic states riding on the Fermi level has been split off by a pseudogap (**FIG. 2(b)**), the electronic structure still keeps a metallic characteristic by GGA + U calculations with a reasonable Coulomb interaction parameter U of 3 eV [52] (**FIG. S1(b)**). Particularly, even much larger U value up to 5 eV is employed, it is still unable to get an insulating gap (see the band structure and corresponding DOS calculated within GGA + U in **FIG. S2(a)** [42]), implying that the correlation effects are insufficient to realize the insulating behavior of Na_2RuO_3 .



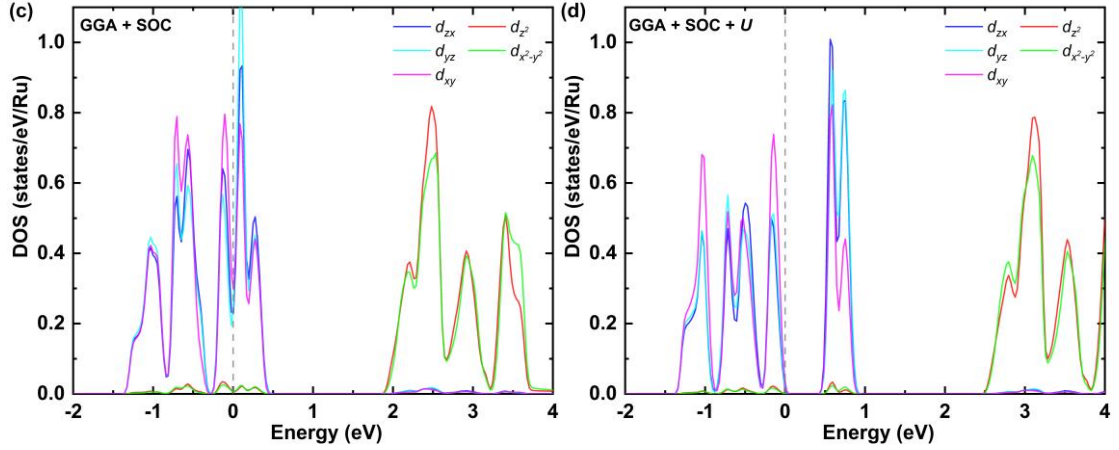


FIG. 2. Comparison of the projected DOS of the 4d state of Ru ions for the nonmagnetic Na_2RuO_3 at ambient pressure calculated by WIEN2K code within: (a) GGA, (b) GGA + U , (c) GGA + SOC and (d) GGA + SOC + U . The Fermi level is set to 0 eV. Only spin-up results are plotted for spin-polarization GGA and GGA + U calculations because the results for the spin-up and spin-down components are identical.

To further explore the underlying effects of SOC on the electronic structure of Na_2RuO_3 , we consider SOC interactions by GGA + SOC calculations. At first glance, SOC interactions don't impose obvious impact on the dispersion of the band structure (see **FIG. S1** for a comparison of the band structures calculated without and with SOC [42]), and the electronic structure essentially remains the metallic characteristic (**FIG. S1(c)** and **FIG. 2(c)**). This result looks reasonable because the atomic SOC strength would be much weaker in the 4d Ru atom (about 0.1 eV) as compared with 5d Ir atom (about 0.4 eV) [53], therefore, the spin-orbit splitting is far less than the t_{2g} bandwidth and is not strong enough to generate a band gap by SOC alone. Interestingly, although individual SOC or U has relatively small influences on the dispersion of the band structures, an insulating gap of ~ 0.6 eV has been opened up around the Fermi level in case SOC together with U are considered simultaneously (**FIG. S1(d)** and **FIG. 2(d)**). The collaborative effect of the onsite Coulomb repulsion U together with SOC points towards an electron-electron correlation enhanced SOC effect [54] as proposed earlier in the 4d transition metal compounds Sr_2RuO_4 [55-57] and Sr_2RhO_4 [58,59], as well as 5d iridates NaIrO_3 [60] and $\beta\text{-Li}_2\text{IrO}_3$ [61]. The correlation-induced enhancement of SOC effect by a factor of about two has been predicted theoretically [55,56] and demonstrated experimentally for Sr_2RuO_4 [57], which plays crucial role in the electronic structure and prominently improves the theoretical description of its Fermi surface. In addition, density matrix

renormalization group and multiorbital dynamical mean-field theory (DMFT) studies indicate that the interplay between Coulomb correlation effect and SOC can realize a nonmagnetic relativistic band insulator in the t_{2g}^4 electron system [9,10].

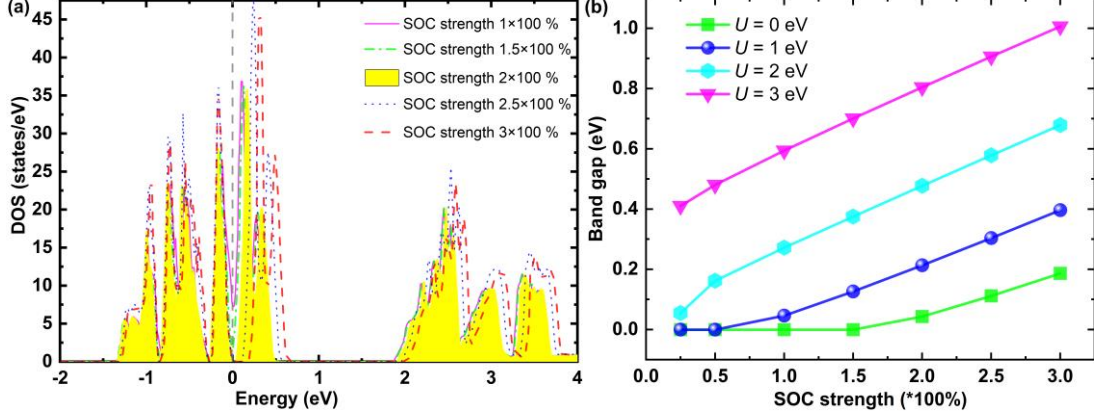


FIG. 3. (a) The evolutions of total DOS of Ru 4d states as a function of SOC strength within GGA+SOC calculations (the opening of insulating gap by enhancing SOC strength to a factor of two has been highlighted), (b) the changes of band gaps as a function of SOC strength as well as Coulomb interaction U within GGA+SOC+ U calculations.

The opening of the nonmagnetic insulating gap in Na_2RuO_3 can be attributed to the enhancement of SOC by correlation effects. We find that just enhance the SOC strength up to two times indeed can open the insulating gap of Na_2RuO_3 without considering the electronic correlation U (**FIG. 3(a)**). In addition, the band gap value further increases linearly along with increasing SOC strength once the gap has been opened (**FIG. S3(a)** [42]), which is consistent with the anticipation that the charge gap is proportional to the SOC strength ($3\lambda/2$) [1]. On the one hand, the insulating gap can be opened by a small Coulomb interaction U of 1 eV if a normal SOC strength has been taken into account, and the band gap increases gradually along with increasing U (**FIG. S3(b)** [42]). On the other hand, along with the increasing Coulomb interaction U , the critical SOC strength to open the band gap gradually decreases from two times (bare SOC without U , $U = 0$) to normal level ($U = 1$ eV) and to 25% ($U = 2$ eV) (**FIG. 3(b)**). Especially, the slope of band gap vs SOC strength increases obviously from 0.143 ($U = 0$ eV) to 0.176 ($U = 1$ eV), 0.203 ($U = 2$ eV) and 0.216 ($U = 3$ eV) along with the Coulomb interaction U increasing from 0 eV to 3 eV, which implies the effective SOC strength λ (derived from the slope, which is equal to $3\lambda/2$) has been enhanced from 0.095 ($U = 0$ eV) to 0.117 ($U = 1$ eV), 0.135 ($U = 2$ eV) and 0.144 ($U = 3$ eV) eV by increasing the electron

correlation (**FIG. S3(b)** [42]). According to our calculation, the effective SOC strength λ is 0.095 eV without U , which has been enhanced up to 0.144 eV by about 1.5 times when $U = 3$ eV. However, without considering Coulomb correction U , the band gap cannot open up even if the SOC strength is enhanced to 1.5 times of the normal value. It should be noted that we are unable to adjust the absolute value of the SOC constants during the simulation, but we can manipulate the relative strength of the SOC, which has been demonstrated to be an effective method to study the $J = 0$ nonmagnetic insulating state of K_2OsX_6 ($X = F, Cl, \text{ and } Br$) with $5d^4$ electronic configuration [49].

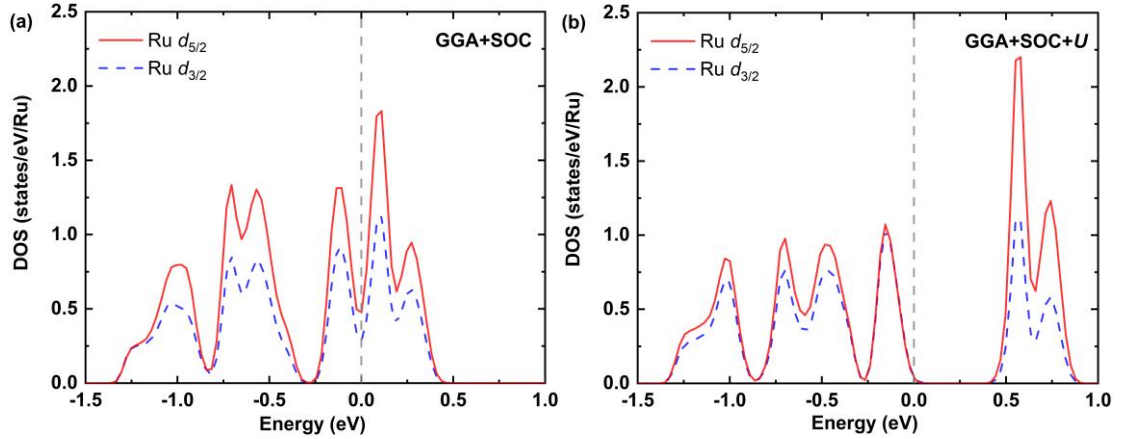


FIG. 4. The Ru 4d DOS projected onto the fully relativistic basis set of Ru $d_{3/2}$ (blue) and $d_{5/2}$ (red) states for Na_2RuO_3 within (a) GGA+SOC and (b) GGA+SOC+ U ($U = 3$ eV).

We have demonstrated that the SOC interactions play a huge impact on the electronic structure of Na_2RuO_3 . Particularly, the combined interplay of electronic correlation with SOC effect has induced the metal-insulator transition (MIT) and nonmagnetic state, which are consistent well with recently experimental results of Na_2RuO_3 [32,37]. However, as shown in **FIG. S1** [42], the individual impact of the SOC effect imposed on the band dispersion of Na_2RuO_3 is not as huge as observed in $5d$ iridates such as $Sr_3M IrO_6$ ($M = Sr, Na, Li$) [21-22], $\beta-Li_2IrO_3$ [61,62] and Ca_4IrO_6 [63], that the SOC interactions are strong enough to cause obvious separation between the $j_{\text{eff}} = 1/2$ and $j_{\text{eff}} = 3/2$ states in these iridates. In order to get further insight to the evolution of the electronic structure of Na_2RuO_3 along with the Coulomb enhanced SOC effect, the projection of Ru 4d states onto the fully relativistic basis set of $d_{3/2}$ and $d_{5/2}$ states is presented in **FIG. 4**. The j_{eff} states can be expressed in terms of $|j, j_z\rangle$ ($j = 5/2, 3/2$) basis (the detailed derivation can be found in the Supplemental Material [42]), the $j_{\text{eff}} = 1/2$ state consists of pure $d_{5/2}$ character and the $j_{\text{eff}} = 3/2$ state has both $d_{5/2}$ and $d_{3/2}$ components in an ideally octahedral environment [3,62,64,65]. However,

without considering the Coulomb correlation, the $j_{\text{eff}} = 1/2$ and $j_{\text{eff}} = 3/2$ states completely mix with each other around the Fermi level, which originates from the weak SOC strength in Na_2RuO_3 together with the octahedral distortion and complicated structural connectivity of the honeycomb lattice [21,65,66]. By contrast, the effective SOC effect is enhanced by Coulomb correlation, the $j_{\text{eff}} = 1/2$ and $j_{\text{eff}} = 3/2$ states are separated by an insulating gap, and the $j_{\text{eff}} = 1/2$ state above Fermi level becomes more dominant while $j_{\text{eff}} = 3/2$ component decreases, providing circumstantial evidence in favor of the j_{eff} picture to describe the electronic structure of Na_2RuO_3 . The Coulomb correlation enhanced SOC effect and resultant MIT in Na_2RuO_3 like the case of iridates NaIrO_3 with $5d^4$ electronic configuration, where the correlation interaction enhances the SOC effect, inducing a band insulating phase with renormalized band structure [60]. In addition, the mechanism of the MIT in Na_2RuO_3 is completely distinct from the SOC assisted Mott MIT in ruthenates and iridates with d^5 electronic configuration, in which the strong SOC effects firstly produce a half-filled $j_{\text{eff}} = 1/2$ states, then the individual Coulomb correlation interactions open a band gap in the $j_{\text{eff}} = 1/2$ states [5].

We remark that the intrinsic nature of the nonmagnetic insulating behavior of Na_2RuO_3 may be different from other insulating d^4 ruthenates such as the honeycomb lattice $\text{Ag}_3\text{LiRu}_2\text{O}_6$ [31] and cubic phase K_2RuCl_6 [36], in which SOC plays a vital role in the formation of SOC entangled $\mathbf{J} = 0$ nonmagnetic singlet according to a LS -coupling scheme [6,7,11]. This spin-orbit entanglement has been proposed as a generic characteristic of the d^4 ruthenates [36], in which both spin and orbital moments should be survived for the LS -coupling induced $\mathbf{J} = 0$ nonmagnetic state. Our calculated results indicate that the spin and orbital moments have completely quenched for the nonmagnetic Na_2RuO_3 , which is inconsistent with the LS -coupling scenario. Alternatively, an itinerant quasi molecular orbitals (QMOs) picture has been proposed to describe the nonrelativistic electronic structure of A_2IrO_3 ($\text{A} = \text{Li}, \text{Na}$) [67-69], RuCl_3 [70] and $\text{Ag}_3\text{LiIr}_2\text{O}_6$ [71]. These compounds feature with d^5 electronic configuration, honeycomb backbone and oxygen assisted d - d hybridizations. SOC effect can destroy the QMO and leads to the formation of the relativistic j_{eff} states. Interestingly, the much smaller SOC effect in RuCl_3 almost plays no impact on the QMOs, but the combination of Coulomb correlation and SOC effect dramatically changes the electronic structure of RuCl_3 , once again providing a hint of the correlation enhanced SOC effect and resultant j_{eff} states [53,70]. Therefore, a low-energy description in terms of relativistic j_{eff} picture may be still valid for Na_2RuO_3 , and the $\mathbf{J} = 0$ nonmagnetic insulating state constructs a basis of the excitonic picture remains to be

confirmed experimentally.

B. Structural dimerization under hydrostatic pressure

In order to inspect whether the hexagonal honeycomb building blocks of Na_2RuO_3 is susceptible to pressure, we simulate the structural stability by applying hydrostatic pressure up to 40 GPa. The evolutions of the crystal structure under compression are summarized in **FIG. 5** and **Tables S6-S8** in the Supplemental Material [42]. As shown in **FIG. 5(a)**, the lattice constants a , b , and c are compressed gradually along with increasing hydrostatic pressure up to 15 GPa, which results in a successive contraction of the cell volume (**FIG. 5(b)**). The response of out-of-plane lattice constant c is greater than those of the in-plane lattice constants a and b (rates of change are $\Delta a \sim 3.02\%$, $\Delta b \sim 3.32\%$, and $\Delta c \sim 5.9\%$, respectively), which is consistent with the layered structure characteristics of Na_2RuO_3 . The lattice parameters undergo remarkable changes once the pressure increases to 17.5 GPa, implying a structural transformation occurs at 15-17.5 GPa. Around 15-17.5 GPa, the lattice constant a only slightly changes, but the lattice constant b experiences a sudden reduction accompanied with an upturn for the lattice constant c , which gives rise in significant shrinkage of volume and monoclinic lattice angle β (**FIG. 5(b)**). Further inspection of the structural detail reveals that the Ru-Ru bond lengths (denoted as X and Y bonds) are almost the same under ambient conditions, which monotonically decrease with pressure, but they change significantly when the pressure exceeds 15 GPa (**FIG. 5(c)**). As shown in **FIG. S4** [42], the Y bond is elongated a bit, whereas the X bond shows an obvious dimerization from 3.00 Å to 2.61 Å, leading to a length difference of about 0.4 Å between the X and Y bonds, the Ru-O bond lengths and O-Ru-O bond angles in the RuO_6 octahedra also change apparently. The structural transition is originated from the dimerization of the Ru-Ru bonds (X bond) along the b axis direction, which is in line with the abrupt shrinking of the in-plane lattice constant b . The bond lengths of the Ru-Ru dimers (2.61 Å) are very close to those of Li_2RuO_3 (2.57 Å) [23] and $\text{Ag}_3\text{LiRu}_2\text{O}_6$ (2.51 Å) [31]. Accompanied by the dimerization of the Ru-Ru bonds, the hexagon of structural units severely deviates from the ideal honeycomb, resulting in distinctly different interior angles (**FIG. 5(d)**).

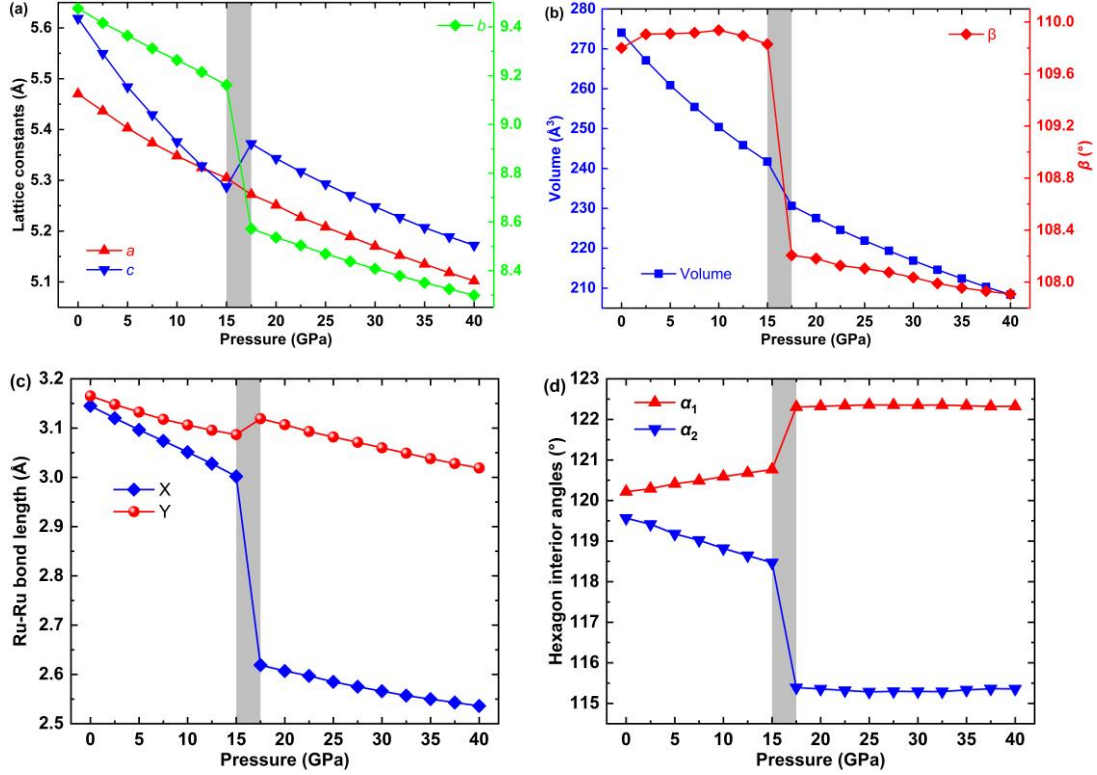


FIG. 5. Evolutions of the crystal structure of the ordered phase Na₂RuO₃ under compression: (a) lattice constants, (b) unit cell volume and the β angle of the monoclinic lattice, (c) Ru-Ru bond lengths, (d) hexagon interior angles. The shadow areas indicate the structural transitions. The data points above 15 GPa are obtained by imposing the $C2/m$ space group.

By a detailed inspection of the structure data at pressure of 17.5 GPa as tabulated in [Table S6](#) in the Supplemental Material [42], we find there is a tiny difference for the Y type Ru-Ru bond lengths, and the hexagon interior angles α_1 and α_2 also show very small differences, respectively. Further structural analysis using the FINDSYM program [72] demonstrates that the new dimerized structure at 17.5 GPa can be assigned to either monoclinic $C2/m$ or $P2_1/m$ space group, depending on the tolerance. The detailed lattice parameters and enthalpies of the high-pressure dimerized phase by imposing these two different space groups are tabulated in [Tables S7](#) and [S8](#) in the Supplemental Material [42]. The calculated equilibrium lattice parameters of the conventional cell are $a = 5.272$ Å, $b = 8.572$ Å, $c = 5.372$ Å, and $\alpha = \gamma = 90^\circ$, $\beta = 108.206^\circ$ for the dimerized monoclinic $C2/m$ phase at 17.5 GPa. By comparison, those of the monoclinic $P2_1/m$ phase are $a = 5.266$ Å, $b = 8.569$ Å, $c = 5.379$ Å, and $\alpha = \gamma = 90^\circ$, $\beta = 108.165^\circ$, respectively. The two structures show very small differences. As shown in [FIG. 6](#), the Y type Ru-Ru bonds are unequal in the $P2_1/m$ phase, and the hexagon interior angles deviate from the ideal 120° with three different values. Despite the

symmetries are different for these two monoclinic structures, the dimerized patterns are the same, which can be named as parallel type [73]. Furthermore, the $P2_1/m$ structure is closely related to the $C2/m$ structure, the monoclinic $P2_1/m$ space group is one of the subgroups of $C2/m$ space group. As shown in **FIG. 6(c)**, the simulated x-ray diffraction patterns of the $C2/m$ and $P2_1/m$ structures are almost identical, indicating it is difficult to distinguish these two high-pressure structures. Further increasing the pressure up to 40 GPa, all lattice parameters change regularly with pressure, which indicates that the dimerized phase of Na_2RuO_3 has been stabilized. The calculated enthalpy of the high-pressure $C2/m$ phase is always comparable to that of the $P2_1/m$ one. The enthalpy differences between $C2/m$ and $P2_1/m$ phases are less than 0.25 meV/atom (**FIG. 6(d)**), which may be within the calculation precision of the VASP code. Therefore, we cannot definitely identify the high-pressure structures of Na_2RuO_3 at present, and hereafter we mainly present the results of the high-pressure dimerized phase with $C2/m$ space group in the main text due to its higher symmetry with respect to the $P2_1/m$ phase.

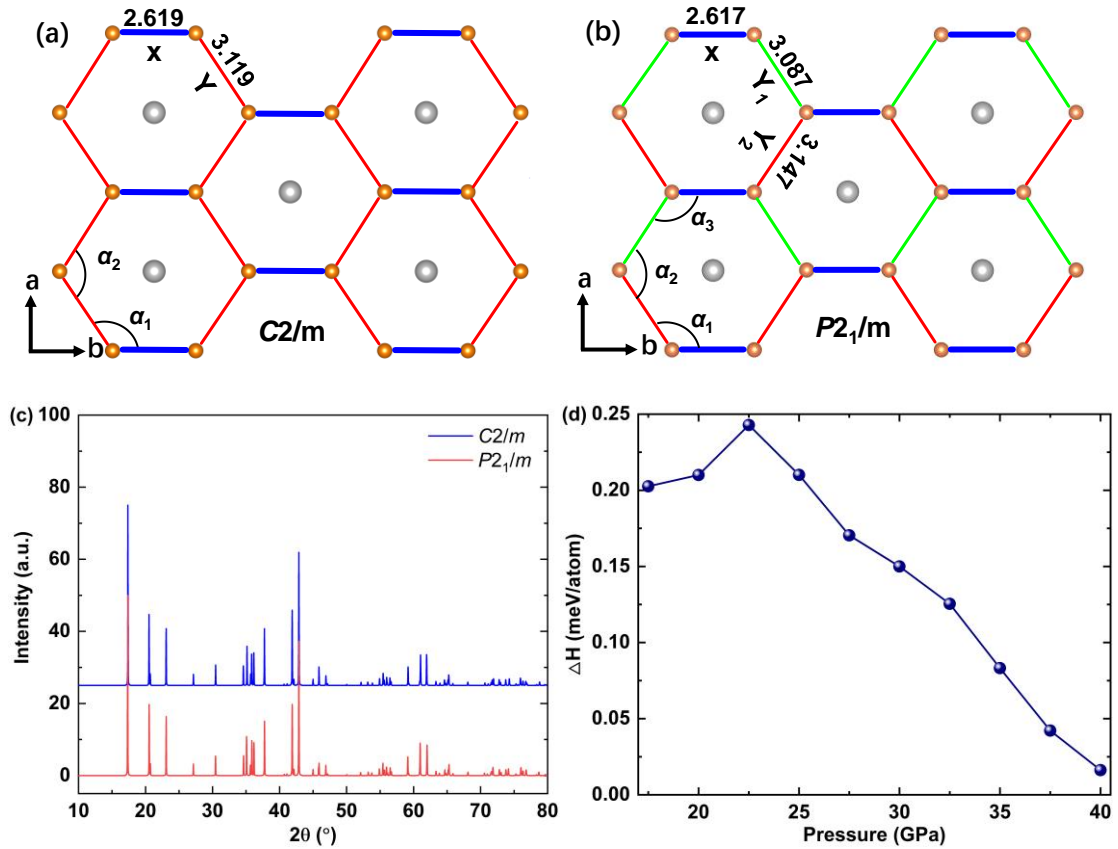


FIG. 6. Schematic diagram of the dimerization patterns of the Ru-Ru bonds in the hexagon formed by edge-sharing RuO_6 octahedra for the crystal structure at 17.5 GPa within (a) $C2/m$ and (b) $P2_1/m$ space group. (c) Simulated x-ray diffraction patterns ($\lambda = 1.541 \text{ \AA}$) of the $C2/m$ and $P2_1/m$ phases

at 17.5 GPa, which are handled by the powder diffraction tool within the Reflex module in Materials Studio program package. (d) The enthalpy differences (ΔH) between the dimerized $C2/m$ and $P2_1/m$ phases along with the increasing pressure.

The lattice structure of the high-pressure dimerized $C2/m$ phase retains the ambient-pressure monoclinic symmetry of Na_2RuO_3 , which is similar to the case of pressure-induced dimerization in Li_2RhO_3 [73]. In contrast, the structure symmetry of the high-pressure dimerized $P2_1/m$ phase of Na_2RuO_3 similar to the case of Li_2RuO_3 , in which the space group has transformed from $C2/m$ to lower-symmetry dimerized $P2_1/m$ along with decreasing temperature ($T_c \sim 550$ K) at ambient pressure [23,25]. Although the structure symmetry shows similarity between Na_2RuO_3 , Li_2RhO_3 and Li_2RuO_3 , the parallel type of dimerization pattern in Na_2RuO_3 differs from the armchair type of dimerization in Li_2RuO_3 induced by temperature decreasing or pressure-induced zigzag chains dimerization in Li_2RhO_3 [23-27, 73]. Different compressive behavior of honeycomb iridates A_2IrO_3 ($A = \text{Na}, \text{Li}$) under pressure has also been uncovered, structural phase transition into a dimerized triclinic phase in Li_2IrO_3 is observed under low pressure, while the $C2/m$ crystal structure of Na_2IrO_3 survive up to very high pressure without dimerization [74-79]. It could speculate that the ionic radii of the buffer elements A in the honeycomb lattice play a significant role in controlling the structure dimerization of A_2IrO_3 ($A = \text{Na}, \text{Li}$) [78,79]. In this context, it is particularly instructive to revisit the compressive behavior of Na_2RuO_3 , the buffer elements also feature distinct ionic radii between Na_2RuO_3 and Li_2RuO_3 . The Na ions occupying the center of the honeycomb plane have larger radius than Li ions, which might realize different dimerization behavior between Na_2RuO_3 and Li_2RuO_3 . Experiments demonstrate that substitution 5% Na for Li has dramatically changed the dimerization pattern of Li_2RuO_3 from the armchair type to zigzag type [27,73]), which can be understood with chemical pressure effects by replacing Li ions with larger-radius Na ions [74]. Various types of pressure-driven dimerization in hexagonal honeycomb systems have been found [73], which are extensively studied in layered honeycomb iridates $\alpha\text{-Li}_2\text{IrO}_3$ [76-79], ruthenate $\text{Ag}_3\text{LiRu}_2\text{O}_6$ [31] and $\alpha\text{-RuCl}_3$ [80-83], respectively. Previous theoretical work predicts that pressure can induce dimerization transition from the monoclinic $C2/m$ phase to a lower-symmetry monoclinic $P2_1/m$ phase for Na_2RuO_3 , the predicted armchair-type dimerization pattern and structure symmetry of the high-pressure phase of Na_2RuO_3 is the same as those of Li_2RuO_3 [41], and the critical pressure of 3 GPa is predicted from the pressure dependence on the volume, which is based on two independent

simulations of the non-dimerized phase and the dimerized phase under compression. However, the structural transition has not been confirmed despite the theory-predicted transition pressure of 3 GPa is easy to implement experimentally. Comparatively, the ambient-condition structure is allowed to freely relax and the structural transition from the non-dimerized phase to the dimerized phase is realized along with the gradual loading of pressure in the present work, which is more like a real high-pressure experiment. A higher transition pressure of 17.5 GPa is predicted in the present work, and the parallel-type dimerized pattern totally differs from the armchair type of dimerization as predicted in previous work [41]. The difference might originate from whether the Coulomb interaction U has been considered, the structural optimization results at ambient condition within GGA+ U are in good agreement with the experimental data, whereas the optimized lattice parameters dramatically deviate from the experimental results when Coulomb interaction U was not considered (see the comparison in **Table S5** in the Supplemental Material [42]). Particularly, the calculation without considering Coulomb interaction U has output obvious short X bonds with respect to the Y bonds (3.027 vs 3.197 Å) and deformed hexagon interior angle. Therefore, previous work may underestimate the transition pressure of the structural dimerization. In view of the higher transition pressure predicted in the present work, it deserves to apply much higher pressure to explore the structural stability of Na₂RuO₃. In addition, recent high-pressure experiment reveals two successive transitions in the $4d^4$ honeycomb ruthenate Ag₃LiRu₂O₆, where the crystal structure of the intermediate phase exhibits the same structure with that at ambient pressure, but the detailed dimerized structure of the higher-pressure phase is still unclear [31]. High quality single crystals and detailed structural characterization are desired to further clarify the complicated dimerization pattern of these honeycomb ruthenates under pressure.

C. Electronic structure transitions under hydrostatic pressure

Previous studies indicate that the structural dimerization in the hexagonal honeycomb materials can lead to a major change of the electronic structure [23-25,31,76-83]. Firstly, we recall the fundamental electronic structure at ambient pressure in **FIG. 2** and the critical role played by the electron-correlation enhanced SOC effect in the nonmagnetic insulating ground state of Na₂RuO₃. Along with the pressure increases to 15 GPa, though the band gap has reduced due to the bandwidth broadening, the essential characteristics of the electronic structure maintain unchanged and the synergistic effects of correlation interactions and SOC still take crucial role in the electronic

structure (FIG. S5 [42]). Once the pressure increases to 17.5 GPa, the structural dimerization is accompanied with a prominent reconstruction of the electronic structure. As shown in FIG. 7 and FIG. S6 [42], the degeneracy of the Ru t_{2g} states in the vicinity of the Fermi level has been completely removed for the high-pressure dimerized phases. The RuO₆ octahedra share edges to form a honeycomb structure, the bond lengths of the dimerized Ru-Ru bonds (X bonds) in Na₂RuO₃ (~ 2.62 Å) are shorter than those in Ru metal (~ 2.7 Å), therefore the overlap between the orbitals becomes larger when the pressure brings the two adjacent Ru ions close enough. Like other dimerized phases of Li₂RuO₃, α -Li₂IrO₃ and α -RuCl₃, the isolated d_{xy} orbitals located in the lowest and highest energy positions of the t_{2g} states, which are separated from the degenerated d_{yz} and d_{zx} orbitals, manifesting strong covalent interactions in the Ru-Ru dimers and the formation of bonding and antibonding states [23,24,76,77,82,83].

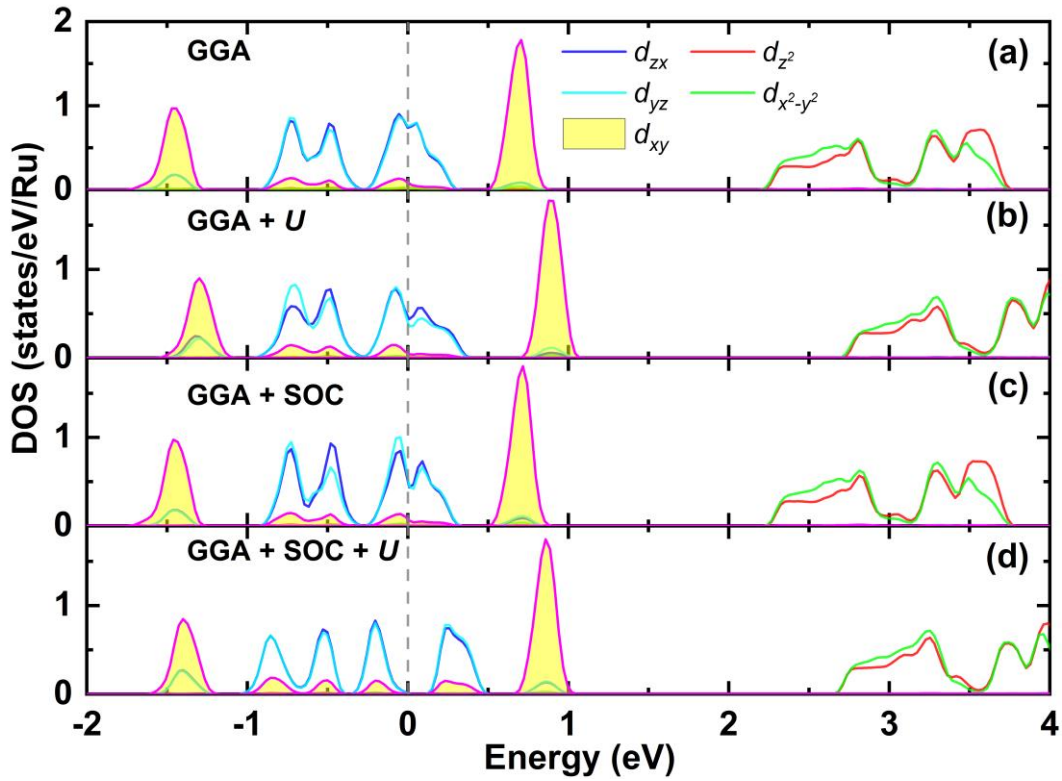


FIG. 7. Projected DOS of the 4d state of Ru ions for the nonmagnetic dimerized Na₂RuO₃ at 17.5 GPa with $C2/m$ space group calculated by WIEN2K code within: (a) GGA, (b) GGA + U , (c) GGA + SOC and (d) GGA + SOC + U . The contributions of the d_{xy} orbitals to the t_{2g} states are highlighted by the shade region. The Fermi level is set to 0 eV. Only spin-up results are plotted for the spin-polarization GGA and GGA + U calculations because the results for the spin-up and spin-down components are identical.

The electronic structure of the dimerized phase can be further analyzed by the real-space wavefunctions in the Ru-Ru dimers. As shown in **FIG. 8**, the d_{xy} orbitals of the two adjacent edge-sharing RuO_6 octahedra form strong bonding and antibonding molecular orbitals (denoted as σ and σ^*) due to the strong enhancement of the direct Ru-Ru hopping path along the dimerized bonds [23,24,77,83-85]. Furthermore, the rest of t_{2g} states, d_{xz} and d_{yz} orbitals also form π and δ types of molecular orbitals in the Ru-Ru dimers. According to this molecular orbital picture, the σ molecular orbitals solely originate from the d_{xy} orbitals, whereas the π and δ types of molecular orbitals consist of linear combinations of $d_{xz}+d_{yz}$ and $d_{xz}-d_{yz}$ orbitals, respectively [24,25,85]. As shown in **FIG. 8** and **FIG. S7** [42], the real-space wavefunctions of the Ru-Ru dimers provide direct evidences of the formation of molecular orbital in the dimerized Na_2RuO_3 . But the bonding and antibonding splitting of the π and δ molecular orbitals are significantly weaker than the σ molecular orbitals, which leads to the broadening of the π and δ states and renders the two states quasi degenerate (**FIG. 7**). Ideally, the eight electrons of the two dimerized Ru^{4+} ions can realize a nonmagnetic electron configuration by filling σ , π and δ bonding orbitals and δ^* antibonding orbitals (considering the spin degree of freedom, each orbital is two-fold degenerate) [23,24,85]. However, the π and δ bonding or antibonding states are slightly split from each other due to the smaller energy difference between them, which obscures the gap due to the band broadening and causes the Fermi level to cut through the doubly degenerate π^*/δ^* antibonding pair as schematic shown in **FIG. 9** [84]. Therefore, the dimerized phase shows a metallic electronic structure even at the level of DFT+ U (**FIG. 7(b)**). Similar to the case of ambient-pressure non-dimerized phase, an increase of the correlation strength up to 5 eV is still unable to open a gap in the degenerate π^*/δ^* antibonding states (**FIG. S2(b)** [42]). In contrast, first-principles DFT calculations and a combination of DFT with the cluster extension of DMFT calculations imply the Coulomb correlation U plays an important role in realizing the insulating state of the low-temperature dimerized phase Li_2RuO_3 [26,86]. Intriguingly, by simultaneously including both Coulomb correlation U and SOC, the degenerated d_{yz} and d_{zx} bands transform into several isolated narrow bands, and an insulating gap has been opened between the π^*/δ^* antibonding states. The MIT in the high-pressure dimerized phase once again implies the crucially collaborative effects of Coulomb correlation U and SOC in Na_2RuO_3 .

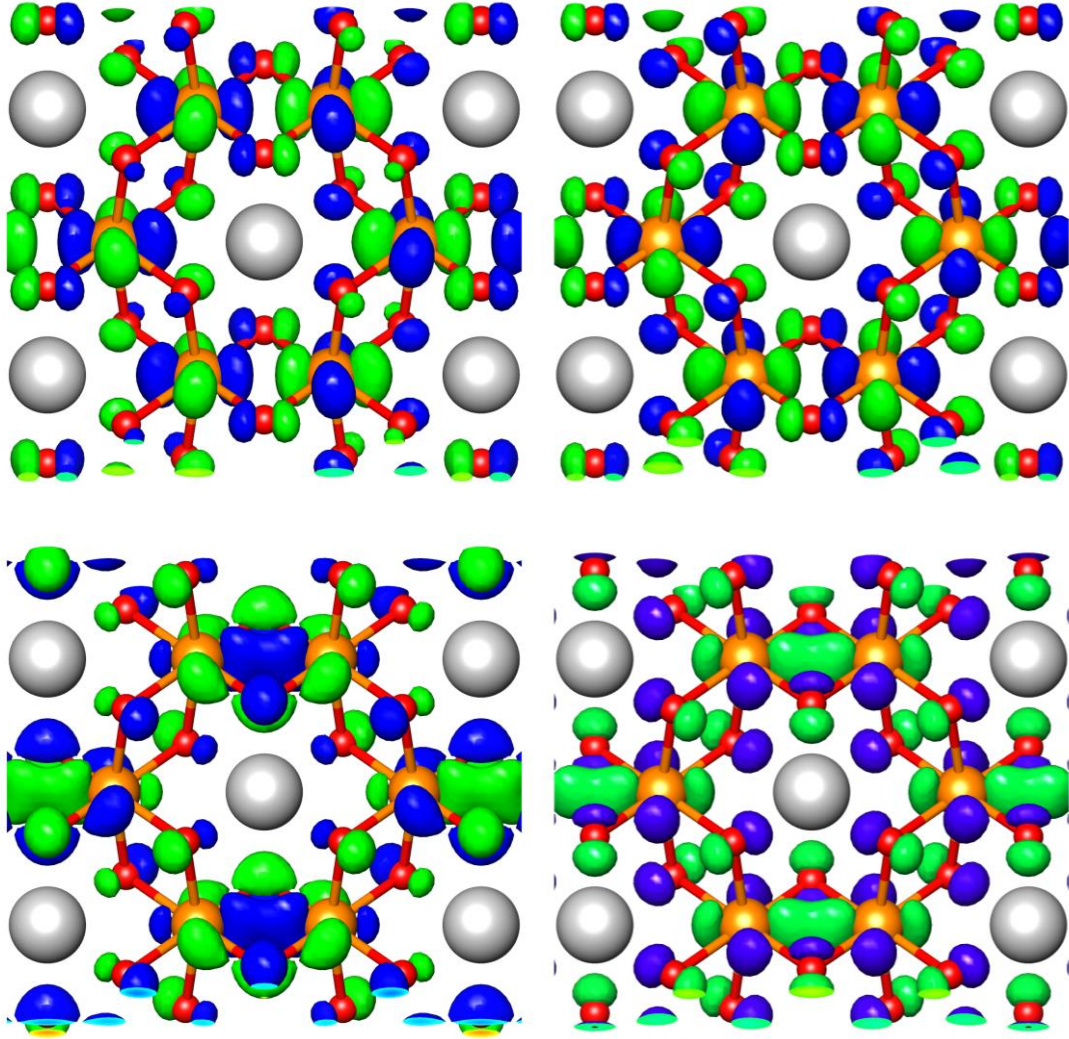


FIG. 8. Real-space visualization of the bonding σ (bottom) and antibonding σ^* (top) molecular orbitals on the Ru-Ru dimers for the nonmagnetic dimerized Na_2RuO_3 at 17.5 GPa with $C2/m$ space group using the VESTA tool [87], the green and blue colors of the isosurfaces denote the positive and negative wave function values, respectively.

Finally, we'd like to summarize the differences between Na_2RuO_3 and Li_2RuO_3 . Firstly, the dimerization of Ru-Ru bonds in Na_2RuO_3 is driven by applied pressure, whereas the dimerization in Li_2RuO_3 is due to temperature decreasing. Secondly, the dimerized phases of Na_2RuO_3 and Li_2RuO_3 show distinct dimerization patterns of parallel and armchair types [23-25]. Thirdly, the Coulomb correlation U and SOC interactions play different role in realizing the insulating state of these ruthenates, while the Coulomb correlation U can open the insulating gap of the dimerized phase Li_2RuO_3 [26,86], whereas only a combination of Coulomb correlation U and SOC effect can

generate the insulating gap of both the ambient-pressure non-dimerized normal phase and the high-pressure dimerized phase of Na_2RuO_3 . In addition, a combination of x-ray diffraction and high-energy x-ray measurements indicate that the dimerized Ru-Ru dimers seem to survive locally in Li_2RuO_3 above the transition temperature, and the high-temperature phase serves as an example of valence bond liquid phase showing orbital-selective metallicity [25,85]. Therefore, it is interesting to clarify the structural details and electronic properties of Na_2RuO_3 under high pressure in further experiments.

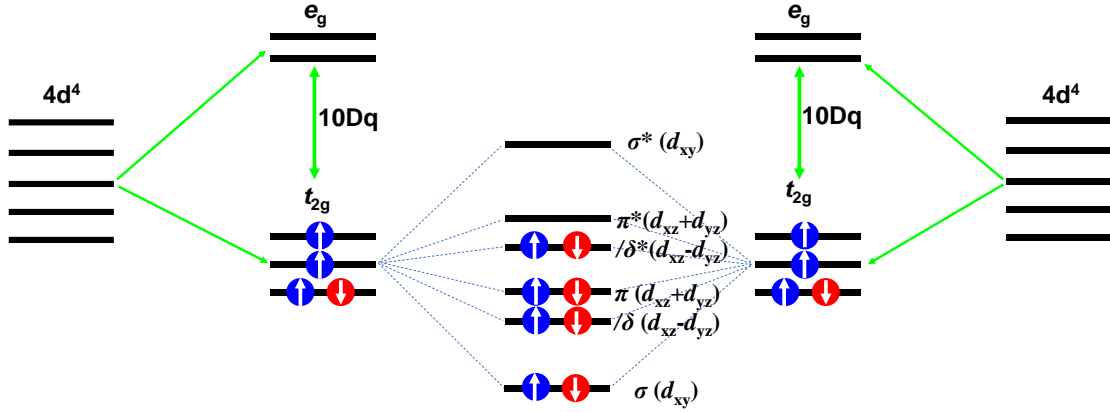


FIG. 9. Schematic diagram of the arrangements of the molecular orbitals and electronic configuration of the Ru-Ru dimers in the dimerized phase Na_2RuO_3 . The d orbitals have been split into two-fold degenerate e_g states and three-fold degenerate t_{2g} states by the octahedral crystal field strength $10Dq$. The strongest bonding σ and antibonding σ^* molecular orbitals occupy the lowest and highest energy levels, while the splitting in the bonding π/δ (antibonding π^*/δ^*) molecular orbitals is not strong enough, giving rise to a mixed state. The arrows directions denote the spin-up and spin-down states.

IV. CONCLUSIONS

In conclusion, we have studied the electronic structure and structural stability of the d^4 ruthenate Na_2RuO_3 by first-principles calculations. The calculated results indicate that the insulating nonmagnetic $J = 0$ ground state of Na_2RuO_3 at ambient conditions is originated from the electron correlation enhanced SOC effect. Furthermore, we discover a pressure-induced structural dimerization of the Ru-Ru bonds featuring with a parallel pattern of the Ru-Ru dimers, which leads to an electronic structure reconstruction by emergence of molecular orbital. Interestingly, Coulomb interactions collaborating with SOC effect can promote the band-gap opening for the nonmagnetic

high-pressure dimerized phase. The crucial role played by the SOC effect in realizing the nonmagnetic insulating behavior of the ambient-pressure non-dimerized phase and high-pressure dimerized phase of Na_2RuO_3 shed new light on the spin-orbital physics, which deserves further theoretical and experimental investigations.

ACKNOWLEDGMENTS

We thank Dr. G. Khaliullin and T. Takayama for fruitful discussions and help. The work was sponsored by the National Natural Science Foundation of China (No. 11864008, 12264011) and Guangxi Natural Science Foundation (No. 2018AD19200 and 2019GXNSFGA245006). C. A. is supported by the Foundation for Polish Science through the International Research Agendas Programme co-financed by EU within the Smart Growth Operational Programme (Grant No. MAB/2017/1). The computational work in this research was carried out at Shanxi Supercomputing Center, and the calculations were performed on TianHe-2.

REFERENCES

- 1 J. G. Rau, E. K.-H. Lee, and H.-Y. Kee, Spin-orbit physics giving rise to novel phases in correlated systems: Iridates and related materials, *Annu. Rev. Condens. Matter Phys.* **7**, 195 (2016).
- 2 W. Witczak-Krempa, G. Chen, Y. B. Kim, and L. Balents, Correlated quantum phenomena in the strong spin-orbit regime, *Annu. Rev. Condens. Matter Phys.* **5**, 57 (2014).
- 3 C. Martins, M. Aichhorn, and S. Biermann, Coulomb correlations in 4d and 5d oxides from first principles—or how spin-orbit materials choose their effective orbital degeneracies, *J. Phys. Condens. Matter* **29**, 263001 (2017).
- 4 R. Schaffer, E. K.-H. Lee, B.-J. Yang and Y. B. Kim, Recent progress on correlated electron systems with strong spin-orbit coupling, *Rep. Prog. Phys.* **79**, 094504 (2016).
- 5 B. J. Kim, H. Jin, S. J. Moon, J.-Y. Kim, B.-G. Park, C. S. Leem, J. Yu, T. W. Noh, C. Kim, S.-J. Oh, J.-H. Park, V. Durairaj, G. Cao and E. Rotenberg, Novel $J_{\text{eff}} = 1/2$ Mott state induced by relativistic spin-orbit coupling in Sr_2IrO_4 , *Phys. Rev. Lett.* **101**, 076402 (2008).
- 6 T. Takayama, J. Chaloupka, A. Smerald, G. Khaliullin, and H. Takagi, Spin-Orbit-Entangled Electronic Phases in 4d and 5d Transition-Metal Compounds, *J. Phys. Soc. Japan* **90**, 062001 (2021).
- 7 S. Bhowal, and I. Dasgupta, Spin-orbit effects in pentavalent iridates: models and materials, *J. Phys. Condens. Matter* **33**, 453001 (2021).
- 8 G. Cao, and P. Schlottmann, The challenge of spin-orbit-tuned ground states in iridates: a key issues review, *Rep. Prog. Phys.* **81**, 042502 (2018).
- 9 N. Kaushal, J. Herbrych, A. Nocera, G. Alvarez, A. Moreo, F. A. Reboredo, and E. Dagotto, Density matrix renormalization group study of a three-orbital Hubbard model with spin-orbit

- coupling in one dimension, Phys. Rev. B **96**, 155111 (2017).
- 10 T. Sato, T. Shirakawa, and S. Yunoki, Spin-orbital entangled excitonic insulator with quadrupole order, Phys. Rev. B **99**, 075117 (2019).
 - 11 G. Khaliullin, Excitonic Magnetism in Van Vleck–type d^4 Mott Insulators, Phys. Rev. Lett. **111**, 197201 (2013).
 - 12 N. Kaushal, J. Herbrych, G. Alvarez, and E. Dagotto, Magnetization dynamics fingerprints of an excitonic condensate t_{2g}^4 magnet, Phys. Rev. B **104**, 235135 (2021).
 - 13 G. Cao, T. F. Qi, L. Li, J. Terzic, S. J. Yuan, L. E. DeLong, G. Murthy, and R. K. Kaul, Novel magnetism of Ir^{5+} ($5d^4$) ions in the double perovskite Sr_2YIrO_6 , Phys. Rev. Lett. **112**, 056402 (2014).
 - 14 L. T. Corredor, G. Aslan-Cansever, M. Sturza, Kaustuv Manna, A. Maljuk, S. Gass, T. Dey, A. U. B. Wolter, Olga Kataeva, A. Zimmermann, M. Geyer, C. G. F. Blum, S. Wurmehl, and B. Büchner, Iridium double perovskite Sr_2YIrO_6 : A combined structural and specific heat study, Phys. Rev. B **95**, 064418 (2017).
 - 15 J. Terzic, H. Zheng, Feng Ye, H. D. Zhao, P. Schlottmann, L. E. De Long, S. J. Yuan, and G. Cao, Evidence for a low-temperature magnetic ground state in double-perovskite iridates with Ir^{5+} ($5d^4$) ions, Phys. Rev. B **96**, 064436 (2017).
 - 16 F. Hammerath, R. Sarkar, S. Kamusella, C. Baines, H.-H. Klauss, T. Dey, A. Maljuk, S. Gaß, A. U. B. Wolter, H.-J. Grafe, S. Wurmehl, and B. Büchner, Diluted paramagnetic impurities in nonmagnetic Ba_2YIrO_6 , Phys. Rev. B **96**, 165108 (2017).
 - 17 T. Dey, A. Maljuk, D. V. Efremov, O. Kataeva, S. Gass, C. G. F. Blum, F. Steckel, D. Gruner, T. Ritschel, A. U. B. Wolter, J. Geck, C. Hess, K. Koepf, J. van den Brink, S. Wurmehl, and B. Büchner, Ba_2YIrO_6 : A cubic double perovskite material with Ir^{5+} ions, Phys. Rev. B **93**, 014434 (2016).
 - 18 S. Fuchs, T. Dey, G. Aslan-Cansever, A. Maljuk, S. Wurmehl, B. Büchner, and V. Kataev, Unraveling the Nature of Magnetism of the $5d^4$ Double Perovskite Ba_2YIrO_6 , Phys. Rev. Lett. **120**, 237204 (2018).
 - 19 A. A. Aczel, Q. Chen, J. P. Clancy, C. dela Cruz, D. Reig-i-Plessis, G. J. MacDougall, C. J. Pollock, M. H. Upton, T. J. Williams, N. LaManna, J. P. Carlo, J. Beare, G. M. Luke, and H. D. Zhou, Spin-orbit coupling controlled ground states in the double perovskite iridates A_2BIrO_6 ($\text{A} = \text{Ba, Sr}$; $\text{B} = \text{Lu, Sc}$), Phys. Rev. Mater. **6**, 094409 (2022).
 - 20 P. Song, Z. Hu, S. Hsu, J. Chen, J. Lee, S. Miao, Y. Shi, and H. L. Feng, Single crystal growth and magnetism of $\text{Sr}_3\text{NaIrO}_6$ and $\text{Sr}_3\text{AgIrO}_6$: Tracking the $J = 0$ ground state of Ir^{5+} , Phys. Rev. Mat. **6**, 094415 (2022).
 - 21 X. Ming, X. Wan, C. Autieri, J. Wen, and X. Zheng, Spin-orbit coupling driven insulating state in hexagonal iridates $\text{Sr}_3\text{M}\text{IrO}_6$ ($M = \text{Sr, Na, Li}$), Phys. Rev. B **98**, 245123 (2018).
 - 22 A. Bandyopadhyay, A. Chakraborty, S. Bhowal, Vinod Kumar, M. M. Sala, A. Efimenko, F. Bert, P. K. Biswas, C. Meneghini, N. Büttgen, I. Dasgupta, T. Saha Dasgupta, A. V. Mahajan,

- and Sugata Ray, Breakdown of atomic spin-orbit coupling picture in an apparently isolated pseudo-one-dimensional iridate: $\text{Sr}_3\text{NaIrO}_6$, *Phys. Rev. B* **105**, 104431 (2022).
- 23 Y. Miura, Y. Yasui, M. Sato, N. Igawa, and K. Kakurai, New-type phase transition of Li_2RuO_3 with honeycomb structure, *J. Phys. Soc. Japan* **76**, 033705 (2007).
 - 24 Y. Miura, M. Sato, Y. Yamakawa, T. Habaguchi, Y. Ono, Structural transition of Li_2RuO_3 induced by molecular-orbit formation, *J. Phys. Soc. Japan* **78**, 094706 (2009).
 - 25 S. A. J. Kimber, I. I. Mazin, J. Shen, H. O. Jeschke, S. V. Streltsov, D. N. Argyriou, R. Valentí, and D. I. Khomskii, Valence bond liquid phase in the honeycomb lattice material Li_2RuO_3 , *Phys. Rev. B* **89**, 081408 (2014).
 - 26 S. Yun, K. H. Lee, S. Y. Park, T.-Y. Tan, J. Park, S. Kang, D. I. Khomskii, Y. Jo, and J.-G. Park, Magnetic and electrical anisotropy with correlation and orbital effects in dimerized honeycomb ruthenate Li_2RuO_3 , *Phys. Rev. B* **100**, 165119 (2019).
 - 27 K. Mehawat and Y. Singh, First-order magnetostructural transition in single crystals of the honeycomb lattice ruthenate Li_2RuO_3 , *Phys. Rev. B* **95**, 075105 (2017).
 - 28 K. M. Mogare, K. Friese, W. Klein, M. J. Prof, Syntheses and crystal structures of two sodium ruthenates: Na_2RuO_4 and Na_2RuO_3 , *Z Anorg Allg Chem* **630**, 547 (2004).
 - 29 J. C. Wang, J. Terzic, T. F. Qi, Feng Ye, S. J. Yuan, S. Aswartham, S. V. Streltsov, D. I. Khomskii, R. K. Kaul, and G. Cao, Lattice-tuned magnetism of Ru^{4+} ($4d^4$) ions in single crystals of the layered honeycomb ruthenates Li_2RuO_3 and Na_2RuO_3 , *Phys. Rev. B* **90**, 161110 (2014).
 - 30 R. Kumar, T. Dey, P. M. Ette, K. Ramesha, A. Chakraborty, I. Dasgupta, J. C. Orain, C. Baines, S. Tóth, A. Shahee, S. Kundu, M. Prinz-Zwick, A. A. Gippius, N. Büttgen, P. Gegenwart, and A. V. Mahajan, Unconventional magnetism in the $4d^4$ -based $S = 1$ honeycomb system $\text{Ag}_3\text{LiRu}_2\text{O}_6$, *Phys. Rev. B* **99**, 054417 (2019).
 - 31 T. Takayama, M. Blankenhorn, J. Bertinshaw, D. Haskel, N. A. Bogdanov, K. Kitagawa, A. N. Yaresko, A. Krajewska, S. Bette, G. McNally, A. S. Gibbs, Y. Matsumoto, D. P. Sari, I. Watanabe, G. Fabbris, W. Bi, T. I. Larkin, K. S. Rabinovich, A. V. Boris, H. Ishii, H. Yamaoka, T. Irifune, R. Bewley, C. J. Ridley, C. L. Bull, R. Dinnebier, B. Keimer, H. Takagi, Competing spin-orbital singlet states in the $4d^4$ honeycomb ruthenate $\text{Ag}_3\text{LiRu}_2\text{O}_6$, *Phys. Rev. Res.* **4**, 043079 (2022).
 - 32 L. S. I. Veiga, M. Etter, E. Cappelli, H. Jacobsen, J. G. Vale, C. D. Dashwood, D. Le, F. Baumberger, D. F. McMorrow, and R. S. Perry, Correlated electron metal properties of the honeycomb ruthenate Na_2RuO_3 , *Phys. Rev. Mater.* **4**, 094202 (2020).
 - 33 V. V. Gapontsev, E. Z. Kurmaev, C. I. Sathish, S. Yun, J.-G. Park and S. V. Streltsov, Spectral and magnetic properties of Na_2RuO_3 , *J. Phys. Condens. Matter* **29**, 405804 (2017).
 - 34 M. Tamaru, X. Wang, M. Okubo, A. Yamada, Layered Na_2RuO_3 as a cathode material for Na-ion batteries, *Electrochemistry Communications* **33**, 23–26 (2013).
 - 35 J. T. Haraldsen, M. B. Stone, M. D. Lumsden, T. Barnes, R. Jin, J. W. Taylor and F. Fernandez-

- Alonso, Spin-lozenge thermodynamics and magnetic excitations in Na_3RuO_4 , *J. Phys.: Condens. Matter* **21**, 506003 (2009).
- 36 H. Takahashi, H. Suzuki, J. Bertinshaw, S. Bette, C. Mühle, J. Nuss, R. Dinnebier, A. Yaresko, G. Khaliullin, H. Gretarsson, T. Takayama, H. Takagi, and B. Keimer, Nonmagnetic $J = 0$ State and Spin-Orbit Excitations in K_2RuCl_6 , *Phys. Rev. Lett.* **127**, 227201 (2021).
- 37 T. Takayama, A. Mukundan, A. Krajewska, D. Le, A. Gibbs and H. Takagi, Magnetic excitations in honeycomb ruthenate Na_2RuO_3 , 2019, <https://data.isis.stfc.ac.uk/doi/STUDY/101225406/>.
- 38 B. M. de Boisse, G. Liu, J. Ma, S. Nishimura, S. Chung, H. Kiuchi, Y. Harada, J. Kikkawa, Y. Kobayashi, M. Okubo and A. Yamada, Intermediate honeycomb ordering to trigger oxygen redox chemistry in layered battery electrode. *Nat. Commun.* **7**, 11397 (2016).
- 39 B. M. de Boisse, M. Reynaud, J. Ma, J. Kikkawa, S. Nishimura, M. C.-Cabanas, C. Delmas, M. Okubo and A. Yamada, Coulombic self-ordering upon charging a large-capacity layered cathode material for rechargeable batteries, *Nat. Commun.* **10**, 2185 (2019).
- 40 L. Clark and A. H. Abdeldaim, Quantum Spin Liquids from a Materials Perspective, *Annu. Rev. Mater. Sci.* **51**, 495 (2021).
- 41 D. D. Gazizova, A. V. Ushakov and S. V. Streltsov, Dimerization in honeycomb Na_2RuO_3 under pressure: a DFT study, *JETP Lett.* **107**, 483 (2018).
- 42 See [Supplemental Material](#) at ***** for detailed derivation of the multiplet splitting arises in the d orbitals, lattice parameters, atomic position and total energy of the ordered phase Na_2RuO_3 for different possible structure at ambient conditions, structural parameters along with the increasing pressure, band structures under ambient conditions, evolution of bond lengths and bond angles, projected DOS for the nonmagnetic dimerized phase at 17.5 GPa with $P2_1/m$ space group, real-space visualization of the molecular orbitals for the nonmagnetic dimerized phase at 17.5 GPa with $C2/m$ space group.
- 43 G. Kresse, and D. Joubert, From ultrasoft pseudopotentials to the projector augmented-wave method, *Phys. Rev. B* **59**, 1758 (1999).
- 44 G. Kresse, and J. Hafner, *Ab initio* molecular dynamics for liquid metals, *Phys. Rev. B* **47**, 558 (1993).
- 45 G. Kresse, and J. Furthmüller, Efficiency of *ab-initio* total energy calculations for metals and semiconductors using a plane-wave basis set, *Comput. Mater. Sci.* **6**, 15 (1996).
- 46 <http://www.wien2k.at>.
- 47 J. P. Perdew, K. Burke, and M. Ernzerhof, Generalized gradient approximation made simple, *Phys. Rev. Lett.* **77**, 3865 (1996).
- 48 A. I. Liechtenstein, V. I. Anisimov, and J. Zaanen, Density-functional theory and strong interactions: Orbital ordering in Mott-Hubbard insulators, *Phys. Rev. B* **52**, 5467(R) (1995).
- 49 Y. Zhang, L. Lin, A. Moreo, and E. Dagotto, $J = 0$ nonmagnetic insulating state in K_2OsX_6 ($X = \text{F}, \text{Cl}, \text{and Br}$), *Phys. Rev. B* **106**, 155148 (2022).

- 50 P. Song, K. Zhu, F. Yang, Y. Wei, L. Zhang, H. Yang, X. Sheng, Y. Qi, J. Ni, S. Li, Y. Li, G. Cao, Z. Y. Meng, W. Li, Y. Shi, and S. Li, Evidence for the random singlet phase in the honeycomb iridate SrIr_2O_6 , *Phys. Rev. B* **103**, L241114 (2021).
- 51 A. de la Torre, B. Zager, J. R. Chamorro, M. H. Upton, G. Fabbris, D. Haskel, D. Casa, T. M. McQueen, and K. W. Plumb, Electronic ground state of two nonmagnetic pentavalent honeycomb iridates, *Phys. Rev. Mater.* **6**, 084406 (2022).
- 52 S. Lee, J.-G. Park, D. T. Adroja, D. Khomskii, S. Streltsov, K. A. McEwen, H. Sakai, K. Yoshimura, V. I. Anisimov, D. Mori, R. Kanno, and R. Ibberson, Spin gap in $\text{Tl}_2\text{Ru}_2\text{O}_7$ and the possible formation of Haldane chains in three-dimensional crystals, *Nat. Mater.* **5**, 471 (2006).
- 53 H.-S. Kim, V. S. V., A. Catuneanu, and H.-Y. Kee, Kitaev magnetism in honeycomb RuCl_3 with intermediate spin-orbit coupling, *Phys. Rev. B* **91**, 241110(R) (2015).
- 54 L. Du, L. Huang and X. Dai, Metal-insulator transition in three-band Hubbard model with strong spin-orbit interaction, *Eur. Phys. J. B* **86**, 1 (2013).
- 55 G. Zhang, E. Gorelov, E. Sarvestani, and E. Pavarini, Fermi Surface of Sr_2RuO_4 : Spin-Orbit and Anisotropic Coulomb Interaction Effects, *Phys. Rev. Lett.* **116**, 106402 (2016).
- 56 M. Kim, J. Mravlje, M. Ferrero, O. Parcollet, and A. Georges, Spin-Orbit Coupling and Electronic Correlations in Sr_2RuO_4 , *Phys. Rev. Lett.* **120**, 126401 (2018).
- 57 A. Tamai, M. Zingl, E. Rozbicki, E. Cappelli, S. Riccò, A. d. I. Torre, S. M. Walker, F. Y. Bruno, P. D. C. King, W. Meevasana, M. Shi, M. Radović, N. C. Plumb, A. S. Gibbs, A. P. Mackenzie, C. Berthod, H. U. R. Strand, M. Kim, A. Georges, and F. Baumberger, High-resolution photoemission on Sr_2RuO_4 reveals correlation-enhanced effective spin-orbit coupling and dominantly local self-energies, *Physical Review X* **9**, 021048 (2019).
- 58 G.-Q. Liu, V. N. Antonov, O. Jepsen, and O. K. Andersen, Coulomb-enhanced spin-orbit splitting: the missing piece in the Sr_2RhO_4 puzzle, *Phys. Rev. Lett.* **101**, 026408 (2008).
- 59 M. W. Haverkort, I. S. Elfimov, L. H. Tjeng, G. A. Sawatzky, and A. Damascelli, Strong Spin-Orbit Coupling Effects on the Fermi Surface of Sr_2RuO_4 and Sr_2RhO_4 , *Phys. Rev. Lett.* **101**, 026406 (2008).
- 60 L. Du, X. Sheng, H. Weng and X. Dai, The electronic structure of NaIrO_3 , Mott insulator or band insulator? *EPL* **101**, 27003 (2013).
- 61 H.-S. Kim, E. K.-H. Lee and Y. Baek, Predominance of the Kitaev interaction in a three-dimensional honeycomb iridate: From ab initio to spin model, *EPL* **112**, 67004 (2016).
- 62 V. N. Antonov, S. Uba, and L. Uba, Electronic structure and x-ray magnetic circular dichroism in the hyperhoneycomb iridate $\beta - \text{Li}_2\text{IrO}_3$, *Phys. Rev. B* **98**, 245113 (2018).
- 63 S. Calder, G.-X. Cao, S. Okamoto, J. W. Kim, V. R. Cooper, Z. Gai, B. C. Sales, M. D. Lumsden, D. Mandrus, and A. D. Christianson, $J_{\text{eff}} = 1/2$ Mott spin-orbit insulating state close to the cubic limit in Ca_4IrO_6 , *Phys. Rev. B* **89**, 081104(R) (2014).
- 64 S. D. Matteo and M. R. Norman, Magnetic ground state of Sr_2IrO_4 and implications for second-

- harmonic generation, Phys. Rev. B **94**, 075148 (2016).
- 65 A. Krajewska, T. Takayama, R. Dinnebier, A. Yaresko, K. Ishii, M. Isobe, and H. Takagi, Almost pure $J_{\text{eff}} = 1/2$ Mott state of $\text{In}_2\text{Ir}_2\text{O}_7$ in the limit of reduced intersite hopping, Phys. Rev. B **101**, 121101 (2020).
- 66 M. A. Tovar-Olvera, Pedro Ruiz-Díaz, and Matthieu Saubanère, Influence of local structural distortion on the magnetism of Na_2IrO_3 compounds, Phys. Rev. B **105**, 094413 (2022).
- 67 I. I. Mazin, H. O. Jeschke, K. Foyevtsova, R. Valentí, and D. I. Khomskii, Na_2IrO_3 as a Molecular Orbital Crystal, Phys. Rev. Lett. **109**, 197201 (2012).
- 68 Y. Li, K. Foyevtsova, H. O. Jeschke, and R. Valentí, Analysis of the optical conductivity for $A_2\text{IrO}_3$ ($A = \text{Na}, \text{Li}$) from first principles, Phys. Rev. B **91**, 161101 (2015).
- 69 K. Foyevtsova, H. O. Jeschke, I. I. Mazin, D. I. Khomskii, and R. Valentí, *Ab initio* analysis of the tight-binding parameters and magnetic interactions in Na_2IrO_3 , Phys. Rev. B **88**, 035107 (2013).
- 70 R. D. Johnson, S. C. Williams, A. A. Haghighirad, J. Singleton, V. Zapf, P. Manuel, I. I. Mazin, Y. Li, H. O. Jeschke, R. Valentí, and R. Coldea, Monoclinic crystal structure of $\alpha\text{-RuCl}_3$ and the zigzag antiferromagnetic ground state, Phys. Rev. B **92**, 235119 (2015).
- 71 Y. Li and R. Valentí, Role of disorder in electronic and magnetic properties of $\text{Ag}_3\text{LiIr}_2\text{O}_6$, Phys. Rev. B **105**, 115123 (2022).
- 72 H. T. Stokes and D. M. Hatch, Program for Identifying the Space Group Symmetry of a Crystal, J. Appl. Cryst. **38**, 237-238 (2005).
- 73 V. Hermann, S. Biswas, J. Ebad-Allah, F. Freund, A. Jesche, A. A. Tsirlin, M. Hanfland, D. Khomskii, P. Gegenwart, R. Valentí, and C. A. Kuntscher, Pressure-induced formation of rhodium zigzag chains in the honeycomb rhodate Li_2RhO_3 , Phys. Rev. B **100**, 064105 (2019).
- 74 V. Hermann, J. Ebad-Allah, F. Freund, I. M. Pietsch, A. Jesche, A. A. Tsirlin, J. Deisenhofer, M. Hanfland, P. Gegenwart, and C. A. Kuntscher, High-pressure versus isoelectronic doping effect on the honeycomb iridate Na_2IrO_3 , Phys. Rev. B **96**, 195137 (2017).
- 75 K. Hu, Z. Zhou, Y. Wei, C. Li, and J. Feng, Bond ordering and phase transitions in Na_2IrO_3 under high pressure, Phys. Rev. B **98**, 100103(R) (2018).
- 76 B. Shen, F. Breitner, D. Prishchenko, R. S. Manna, A. Jesche, M. L. Seidler, P. Gegenwart, and A. A. Tsirlin, Pressure-induced dimerization and collapse of antiferromagnetism in the Kitaev material $\alpha\text{-Li}_2\text{IrO}_3$, Phys. Rev. B **105**, 054412 (2022).
- 77 J. P. Clancy, H. Gretarsson, J. A. Sears, Y. Singh, S. Desgreniers, K. Mehlawat, S. Layek, G. Kh. Rozenberg, Y. Ding, M. H. Upton, D. Casa, N. Chen, J. Im, Y. Lee, R. Yadav, L. Hozoi, D. Efremov, J. v. d. B. and Y.-J. Kim, Pressure-driven collapse of the relativistic electronic ground state in a honeycomb iridate, npj Quant Mater **3**, 35 (2018).
- 78 V. Hermann, M. Altmeyer, J. Ebad-Allah, F. Freund, A. Jesche, A. A. Tsirlin, M. Hanfland, P. Gegenwart, I. I. Mazin, D. I. Khomskii, R. Valentí, and C. A. Kuntscher, Competition between spin-orbit coupling, magnetism, and dimerization in the honeycomb iridates: $\alpha\text{-Li}_2\text{IrO}_3$ under

- pressure, Phys. Rev. B **97**, 020104 (2018).
- 79 S. Layek, K. Mehawat, D. Levy, E. Greenberg, M. P. Pasternak, J.-P. Itié, Y. Singh, and G. Kh. Rozenberg, Electronic and structural properties of the honeycomb iridates $A_2\text{IrO}_3$ ($A = \text{Na}, \text{Li}$) at elevated pressures, Phys. Rev. B **102**, 085156 (2020).
- 80 Z. Wang, J. Guo, F. F. Tafti, A. Hegg, S. Sen, V. A. Sidorov, L. Wang, S. Cai, W. Yi, Y. Zhou, H. Wang, S. Zhang, K. Yang, A. Li, X. Li, Y. Li, J. Liu, Y. Shi, W. Ku, Q. Wu, R. J. Cava, and L. Sun, Pressure-induced melting of magnetic order and emergence of a new quantum state in $\alpha\text{-RuCl}_3$, Phys. Rev. B **97**, 245149 (2018).
- 81 Y. Cui, J. Zheng, K. Ran, J. Wen, Z.-X. Liu, B. Liu, W. Guo, and W. Yu, High-pressure magnetization and NMR studies of $\alpha\text{-RuCl}_3$, Phys. Rev. B **96**, 205147 (2017).
- 82 G. Bastien, G. Garbarino, R. Yadav, F. J. Martinez-Casado, R. B. Rodríguez, Q. Stahl, M. Kusch, S. P. Limandri, R. Ray, P. Lampen-Kelley, D. G. Mandrus, S. E. Nagler, M. Roslova, A. Isaeva, T. Doert, L. Hozoi, A. U. B. Wolter, B. Büchner, J. Geck, and J. van den Brink, Pressure-induced dimerization and valence bond crystal formation in the Kitaev-Heisenberg magnet $\alpha\text{-RuCl}_3$, Phys. Rev. B **97**, 241108 (2018).
- 83 T. Biesner, S. Biswas, W. Li, Y. Saito, A. Pustogow, M. Altmeyer, A. U. B. Wolter, B. Büchner, M. Roslova, T. Doert, S. M. Winter, R. Valentí, and M. Dressel, Detuning the honeycomb of $\alpha\text{-RuCl}_3$: Pressure-dependent optical studies reveal broken symmetry, Phys. Rev. B **97**, 220401(R) (2018).
- 84 M. D. Johannes, A. M. Stux, and K. E. Swider-Lyons, Electronic structure and properties of Li-insertion materials: Li_2RuO_3 and RuO_2 , Phys. Rev. B **77**, 075124 (2008).
- 85 P. McArdle, F. Huang, J. Yang, M. Chu, S. Cheong, and M. M. Qazilbash, Orbital-selective metallicity in the valence-bond liquid phase of Li_2RuO_3 , Phys. Rev. B **105**, 245148 (2022).
- 86 Z. V. Pchelkina, A. L. Pitman, A. Moewes, E. Z. Kurmaev, Teck-Yee Tan, D. C. Peets, Je-Geun Park, and S. V. Streltsov, Electronic structure of Li_2RuO_3 studied by LDA and LDA+DMFT calculations and soft X-ray spectroscopy, Phys. Rev. B **91**, 115138 (2015).
- 87 K. Momma and F. Izumi, VESTA 3 for three-dimensional visualization of crystal, volumetric and morphology data, J. Appl. Cryst. **44**, 1272 (2011).